Electronic structure of $PrNiO_3$ studied by photoemission and x-ray-absorption spectroscopy: Band gap and orbital ordering

T. Mizokawa and A. Fujimori
Department of Physics, University of Tokyo, Bunkyo-ku, Tokyo 113, Japan

T. Arima and Y. Tokura
Department of Applied Physics, University of Tokyo, Bunkyo-ku, Tokyo 113, Japan

N. Mōri
Institute for Solid State Physics, University of Tokyo, Minato-ku, Tokyo 113, Japan

J. Akimitsu
Department of Physics, College of Science and Engineering, Aoyama-Gakuin University, Setagaya-ku, Tokyo 157, Japan
(Received 10 May 1995; revised manuscript received 30 June 1995)

The electronic structure of $PrNiO_3$ has been studied by photoemission and x-ray-absorption spectroscopy. By analyzing the spectra using configuration-interaction calculations on a NiO_6 cluster model, it has been found that the charge-transfer energy Δ is ~ 1 eV and the Ni $3d$ and O $2p$ orbitals are strongly hybridized in the ground state. From the cluster-model calculation, the magnetic moment of Ni $3d$ is estimated to be $\sim 0.9\mu_B$, which is close to the ionic value of Ni^{3+} and in good agreement with that obtained from neutron-diffraction experiments. Using the electronic-structure parameters deduced from the cluster-model analysis, we have performed unrestricted Hartree-Fock calculations on a Ni $3d$–O $2p$ perovskite-type lattice model in order to study the effect of $GdFeO_3$-type distortion on the orbital polarization and band gap.

I. INTRODUCTION

Perovskite-type $3d$ transition-metal oxides, which exhibit various physical properties, are very fascinating systems. One of them, $RNiO_3$ (R = rare earth), shows a metal-insulator transition as a function of the size of the rare-earth ion or of the Ni-O-Ni bond angle.[1] While the least distorted $LaNiO_3$, which has the rhombohedral structure, is a paramagnetic (PM) metal,[2] more distorted $RNiO_3$ with a smaller R ion than La has the orthorhombic $GdFeO_3$-type structure (Fig. 1) and becomes an antiferromagnetic (AFM) insulator.[1] Some orthorhombic $RNiO_3$ with an R ion of intermediate size show a metal-insulator transition as a function of temperature. The transition temperature increases as the R ion becomes smaller.[1] In addition to the metallic versus insulating behavior, the magnetic structures of AFM $PrNiO_3$ and $NdNiO_3$ were found to be very complicated and to indicate the existence of orbital ordering.[3] In order to reveal the origin of the electrical and magnetic properties of $RNiO_3$, it is very important to investigate its electronic structure.

The electronic structures of the $3d$ transition-metal compounds have been interpreted in the framework of the Zaanen-Sawatzky-Allen (ZSA) scheme,[4] where the transition-metal compounds are classified into two regimes, namely, the Mott-Hubbard regime and the charge-transfer regime. In the Mott-Hubbard regime, the $3d$-$3d$ Coulomb repulsion energy U is smaller than the ligand-to-metal charge-transfer energy Δ and the magnitude of the band gap is given by $\sim U$. In the charge-transfer regime, where $\Delta < U$, the magnitude of the gap is determined by Δ. Recently, it has been pointed out that the electronic structures of high-valence oxides such as Cu^{3+}, Ni^{3+}, and Fe^{4+} oxides are characterized by a small or even negative charge-transfer energy and the magnitude of the band gap is determined by the transition-metal $3d$–oxygen $2p$ hybridization and hence is strongly affected by the geometrical arrangement of the transition-metal and oxygen ions.[5] In these compounds, therefore, a small lattice distortion may cause a metal-insulator transition.

$RNiO_3$ is a candidate for this kind of compound and some studies have been done trying to understand its electronic structure. From neutron-diffraction measurements on $PrNiO_3$ and $NdNiO_3$, García-Muños, Rodríguez-Carvajal, and Lacorre have shown that the ordered magnetic moment at the Ni site is $\sim 0.9\mu_B$, which is close to the purely ionic value $1\mu_B$ of Ni^{3+} and has been taken as evidence for the ionic character of $RNiO_3$.[3] Medarde *et al.* have performed x-ray-absorption spectroscopy (XAS) of $RNiO_3$ and have also concluded that the ground state has mainly d^7 character.[6] Very recently, Barman, Chainani, and Sarma have reported the photoemission spectroscopy study of $LaNiO_3$ and $NdNiO_3$. They claimed that the difference between the metallic $LaNiO_3$ and the insulating $NdNiO_3$ is driven by the difference in the transition-metal $3d$–to–oxygen $2p$ transfer integrals within the NiO_6 cluster.[7] In this paper, we have investigated the electronic structure of $PrNiO_3$

0163-1829/95/52(19)/13865(9)/$06.00

using photoemission and XAS measurements and subsequent cluster-model calculations. It has been found that the d^7 and $d^8\underline{L}$ configurations are strongly mixed in the ground state and that this does not contradict a magnetic moment close to the ionic value. Unrstricted Hartree-Fock (HF) calculations have also been performed on a Ni $3d$–O $2p$ perovskite-type lattice model using the electronic-structure parameters deduced from the cluster-model analysis in order to investigate the relationship between the $GdFeO_3$-type lattice distortion and the metal-insulator transition of $RNiO_3$. It has been shown that the $GdFeO_3$-type distortion increases the magnitude of the band gap of $RNiO_3$.

The organization of this paper is as follows. Experimental details are presented in Sec. II. The methods of the cluster-model and unrestricted Hartree-Fock calculations are described in Sec. III. In Sec. IV, photoemission spectra and XAS spectra are displayed and are analyzed by the calculations.

II. EXPERIMENTS

Polycrystalline samples of $PrNiO_3$ were prepared by solid-state reaction under high oxygen pressure. The starting material was prepared by dissolving Pr_6O_{11} and NiO in concentrated nitric acid. The excess nitric acid was removed by heating it to 200 °C in air. The remaining intimately mixed nitrates were decomposed to black powders at 800 °C in an O_2 atmosphere. After grinding, the powders were sealed in a platinum capsule with $KClO_3$ and prssurized under 5 GPa using a cubic anvil high-pressure apparatus. Heat treatment under pressure was carried out at 1300 °C for 1 h.[8]

Photoelectrons were collected with a Physical Electronics double-pass cylindrical-mirror analyzer for both x-ray photoemission spectroscopy (XPS) and ultraviolet photoemission spectroscopy (UPS). A Mg $K\alpha$ x-ray source ($h\nu=1253.6$ eV) was used for the XPS measurements. The XPS spectra were corrected for the Mg $K\alpha_{3,4}$ ghost. The energy resolution including both the x-ray source and the analyzer was ~1.0 eV. UPS spectra including Ni $3p$-$3d$ resonant photoemission spectra were measured at beamline BL-2 of Synchrotron Radiation Labortory, Institute for Solid State Physics, University of Tokyo. The energy resolution was 0.3–0.5 eV for the photon energy ranging from 40 to 100 eV. All the photoemission measurements were made at liquid-nitrogen temperature. In order to obtain fresh surfaces, the samples were scraped with a diamond file under an ultrahigh vacuum (UHV) of low 10^{-10} Torr until the O $1s$ core-level spectra became a single peak. The XAS spectra have been measured at beamline BL-2B of Photon Factory, Laboratory for High Energy Physics. The measurement has been done at room temperature in the total-electron-yield mode. Since the XAS measurement is also sensitive to surface contamination, the samples were scraped under an UHV of low 10^{-9} Torr. The energy resolution was ~0.2 eV at 530 eV. The photon energy was calibrated using the O $1s$ edge of TiO_2 at 530.7 eV,[9] and the Cu $2p_{3/2}$ edge of Cu metal at 932.5 eV.[10]

III. METHOD OF MODEL CALCULATIONS

A. Cluster-model calculations

We have analyzed the photoemissin and x-ray-absorption spectra using configuration-interaction (CI) calculations on an octahedral NiO_6 cluster model (with O_h symmetry).[11,12] The wave functions for the cluster are spanned by basis functions of the ionic configuration d^n and the charge-transferred configurations $d^{n+m}\underline{L}^m$, where $\underline{L}$ denotes an oxygen $2p$ hole. The wave function of the ground state or the N-electron system is given by

$$\Psi_g=a_0|d^7\rangle+a_1|d^8\underline{L}\rangle+a_2|d^9\underline{L}^2\rangle \ . \tag{1}$$

The oxygen $2p$–to–Ni $3d$ charge-transfer energy is defined by $\Delta\equiv E(d^8\underline{L})-E(d^7)$ and the $3d$-$3d$ Coulomb interaction energy by $U\equiv E(d^6)+E(d^8)-2E(d^7)$, where $E(d^n\underline{L}^m)$ is the center of gravity of the $d^n\underline{L}^m$ multiplets or the average of all the terms in the multiplets including the degeneracies. The final states of $3d$ photoemission or the $(N-1)$-electron states are expressed by

$$\Psi_f=b_0|d^6\rangle+b_1|d^7\underline{L}\rangle+b_2|d^8\underline{L}^2\rangle \ . \tag{2}$$

The energy differences $E(d^7\underline{L})-E(d^6)$ and $E(d^8\underline{L}^2)-E(d^7\underline{L})$ are $\Delta-U$ and Δ, respectively. Corresponding $3d$ photoemission intensities are given by $|a_0b_0+a_1b_1+a_2b_2|^2$ in the sudden approximation. In the same way, the wave functions of the $(N+1)$-electron states are written as

$$\Psi_f=c_0|d^8\rangle+c_1|d^9\underline{L}\rangle+c_2|d^{10}\underline{L}^2\rangle \ . \tag{3}$$

These can be regarded as the final states of O $1s$ XAS if we neglect interaction between an O $1s$ core hole and Ni $3d$ electrons. Their intensities are proportional to $|a_1c_0+a_2c_1|^2$.

The final states of Ni $2p$ core-level photoemission are given by

$$\Psi_f=d_0|\underline{c}d^7\rangle+d_1|\underline{c}d^8\underline{L}\rangle+d_2|\underline{c}d^9\underline{L}^2\rangle+d_3|\underline{c}d^{10}\underline{L}^3\rangle \ , \tag{4}$$

where $\underline{c}$ denotes a Ni $2p$ core hole. When the Coulomb interaction between a Ni $2p$ hole and a Ni $3d$ hole is denotes by Q, the energy differences $E(\underline{c}d^8\underline{L})-E(\underline{c}d^7)$ and $E(\underline{c}d^9\underline{L}^2)-E(\underline{c}d^8\underline{L})$ are $\Delta-Q$ and $\Delta-Q+U$, respectively. The $2p$ core-level photoemission intensities are given by $|a_0d_0+a_1d_1+a_2d_2|^2$. For Ni $2p$ XAS, the final states are expressed by

$$\Psi_f=e_0|\underline{c}d^8\rangle+e_1|\underline{c}d^9\underline{L}\rangle+e_2|\underline{c}d^{10}\underline{L}^2\rangle \ , \tag{5}$$

whose intensities are proportional to $|a_0e_0+a_1e_1+a_2e_2|^2$.

In the cluster-model calculations for the valence-band spectra, we have three adjustable parameters which are to be determined to reproduce the experimental results: Δ, U, and the transfer integrals between the Ni $3d$ and O $2p$ orbitals. The transfer integrals are expressed in terms of Slater-Koster parameters $(pd\sigma)$ and $(pd\pi)$.[13] The ratio $(pd\sigma)/(pd\pi)$ is fixed to be ~-2.2,[14,15] and only $(pd\sigma)$ is taken as an adjustable parameter. The multiplet split-

ting of d^n configurations is taken into account through Racah parameters, B and C, which have been fixed to the free-ion values.[16,17] The multiplet-averaged $3d$-$3d$ Coulomb interaction U and charge-transfer energy Δ for d^n are given by $A-14/9B+7/9C$ and $\varepsilon_d^0-\varepsilon_p+nU$, respectively, where ε_d^0 and ε_p are the bare energy levels of the $3d$ and $2p$ orbitals. For the Ni $2p$ core-level spectra, the Coulomb interaction between the Ni $2p$ hole and the Ni $3d$ hole Q is added to the above three adjustable parameters. From previous cluster-model analyses, it has been empirically found that the ratio U/Q should be 0.7–0.9.[12,18,19] In the present calculation, the ratio U/Q is assumed to be 0.8. When we tentatively varied the ratio within the above range, agreement with experimental results were not improved significantly. The multiplet coupling between the Ni $2p$ core hold and the Ni $3d$ holes is included through Slater integrals F^2, G^1, and G^3, which are also fixed to the free-ion values.[17,20]

We have included the crystal-field splitting $10Dq$ which arises from the nonorthogonality between the atomic oxygen $2p$ and transition-metal $3d$ orbitals.[16,21] The overlap integrals can be deduced from the linear-combination-of-atomic-orbitals (LCAO) fitting of the band-structure calculations by Mattheiss.[15] We have assumed the ratio of the overlap integrals S_σ and S_π to the transfer integrals $(pd\sigma)$ and $(pd\pi)$ to be ~ -0.06 eV^{-1}. The $10Dq$ from the nonorthogonality is given by $-2(V_eS_e-V_{t2}S_{t2})$, where $V_e=-\sqrt{3}(pd\sigma)$, $S_3=-\sqrt{3}S_\sigma$, $V_{t2}=2(pd\pi)$, and $S_{t2}=2S_\pi$.

In general, it is hard to reproduce both the valence-band and core-level photoemission spectra using the same parameter set in the cluster-model calculations because the final states have different numbers of $3d$ electrons and core holes. In this work, configuration dependence of the transfer integral has been taken into account to make it possible to reproduce the valence-band and Ni $2p$ core-level XPS spectra with the same parameter set. Following Gunnarsson and Jepsen,[22] we have assumed that the transfer integrals between $d^{n-1}\underline{L}^m$ and $d^n\underline{L}^{m+1}$ are 80% of those between $d^n\underline{L}^m$ and $d^{n+1}\underline{L}^{m+1}$ and that those between $\underline{c}d^n\underline{L}^m$ and $\underline{c}d^{n+1}\underline{L}^{m+1}$ are 70% of those between $d^n\underline{L}^m$ and $d^{n+1}\underline{L}^{m+1}$.[21]

B. Unrestricted Hartree-Fock calculations

In order to study the effect of translational symmetry, we have performed unrestricted HF calculations on the perovskite-type Ni $3d$–O $2p$ lattice.[23] The unrestricted HF approximation is a powerful tool to study spin- and orbital-ordered insulating states in the lattice model. Cyrot and Lyon-Caen have made HF calculations on a doubly degenerate Hubbard model and found that the ferromagnetic (FM) state with orbital ordering is favored.[24] Recently, HF calculations have been made for the CuO_2 plane, where there is no degeneracy in the $3d$ obital, to study the metal-insulator boundary in the ZSA diagram.[25] This study has shown that the HF approximation is useful to investigate metal-insulator transitions.

In our model, the intra-atomic $3d$-$3d$ Coulomb interaction is taken into account in terms of Kanamori parameters u, u', j, and j', for which the relationships

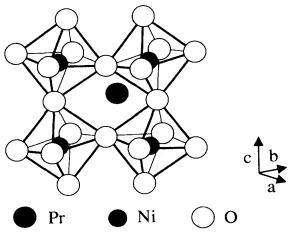

FIG. 1. Simplified structure of the $GdFeO_3$-type lattice. The Ni-O-Ni bond angle decreases from 180° as the distortion increases.

$u'=u-2j$ and $j'=j$ are assumed.[26] These Kanamori parameters can be related to Racah prameters through $u=A+4B+3C$ and $j=\frac{5}{2}B+C$. The multiplet-averaged $3d$-$3d$ Coulomb interaction U and charge-transfer energy Δ for the d^n configuration are given by $u-\frac{20}{9}j$ and $\varepsilon_d^0-\varepsilon_p+nU$, respectively.

Our criterion for the self-consistency of the HF calculation is that all the differences of the order parameters in the subsequent iteration steps are less than 1×10^{-3}. We have taken 512 **k** points in the first Brillouin zone for the $GdFeO_3$ structure, whose unit cell has four Ni sites, and 64 **k** points for the actual magnetic structure of $PrNiO_3$, whose unit cell contains 16 Ni sites. In the present calculations, the $GdFeO_3$-type distortion of $PrNiO_3$ is imitated by rotating the NiO_6 octahedra of the cubic perovskite structure around the a axis of the $GdFeO_3$ structure (see Fig. 1).

IV. RESULTS AND DISCUSSION

A. Core-level XPS

In Fig. 2, we have plotted the XPS spectrum of the O $1s$ core level which overlaps with the Pr MNN Auger spectrum. The O $1s$ peak at 528.3 eV is almost a single peak, which shows the cleanness of the surface. The broad structure at ~531 eV may be derived from surface contamination superposed on the Pr MNN emission. The amount of contamination is small enough for us to

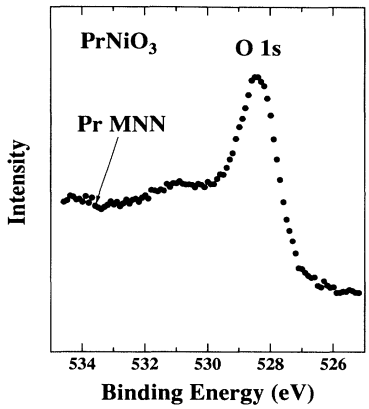

FIG. 2. O $1s$ XPS spectrum of $PrNiO_3$. The spectrum has been corrected for the Mg $K\alpha_{3,4}$ satellites.

analyze the following spectra and to extract information on the electronic structure of $PrNiO_3$.

As shown in Fig. 3, the Ni $2p$ core-level XPS spectrum has satellite structures, which have been generally observed in late transition-metal oxides. We have analyzed the Ni $2p$ core-level spectrum using the CI cluster model with and without multiplet effects. The Ni $2p$ spectra calculated without the multiplet effect are compared with the experimental results in the upper panel of Fig. 3. Here, we have broadened the line spectra by a Lorentzian, the full width at half maximum (FWHM) of which is proportional to the energy separation from the main peak.[18] In calculating the Ni $2p$ core-level spectrum, Q is assumed to be $\sim U/0.8$ as before.[18] With U and Q being fixed at 7 and 9 eV, respectively, the best fit has been obtained for $\Delta=1\pm1$ eV and $(pd\sigma)=-1.5\pm0.2$ eV. The final states are decomposed into $\underline{c}d^7$, $\underline{c}d^8\underline{L}$, $\underline{c}d^9\underline{L}^2$, and $\underline{c}d^{10}\underline{L}^3$ components in the lower panel of Fig. 3. The main peaks and the satellite structures have $\underline{c}d^9\underline{L}^2$ and $\underline{c}d^8\underline{L}$ character, respectively. The amount of $d^{10}\underline{L}^3$ in the main peak is not negligible since Δ is smaller than Q-U in the present calculation.

We have also performed cluster-model calculations for the Ni $2p$ spectrum by fully taking the intra-atomic multiplet coupling into account. When all the configurations up to $d^{10}\underline{L}^3$ are included, the number of bases becomes very large (6820). Since numerical diagonalization of such a large matrix is impossible, we have employed the Lanczos method.[27] However, the size of the calculation is still so huge that we could not do iterative calculations to find the best-fit parameter set. Here, we have done the calculation using the same parameter set as that obtained without the multiplet effect. Since the satellite structures are broadened by the multiplet splittings, there is no need to apply the extra broadening for the satellite part although the inclusion of a weak Lorentzian broadening somewhat improves agreement between experiment and calculation. The calculated result using $\Delta=1$ eV, $U=7$ eV, and $(pd\sigma)=-1.5$ eV is compard with the experimental result in Fig. 4. The Slater integrals between the Ni $2p$ and $3d$ orbitals are $F^2=6.68$, $G^1=5.07$, and $G^3=2.88$ eV. The multiplet-averaged $2p$-$3d$ Coulomb interaction $Q(\equiv F^0-\frac{1}{15}G^1-\frac{3}{70}G^3)$ is ~9.0 eV. The Racah

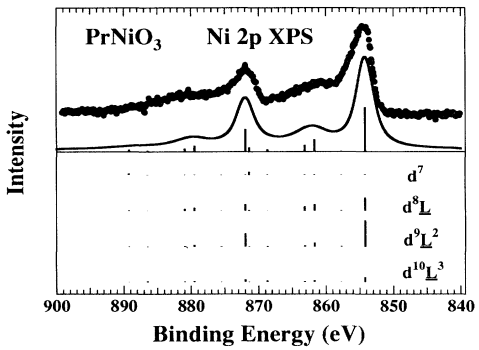

FIG. 3. Ni $2p$ XPS spectrum of $PrNiO_3$ compared with the cluster-model calculation without multiplet coupling (upper panel). The line spectra are decomposed into the d^7, $d^8\underline{L}$, $d^9\underline{L}^2$, and $d^{10}\underline{L}^3$ components (lower panel).

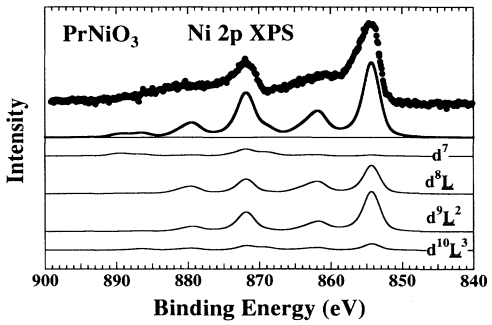

FIG. 4. Ni $2p$ XPS spectrum of $PrNiO_3$ compared with the cluster-model calculation with multiplet coupling (upper panel). The line spectra are decomposed into the d^7, $d^8\underline{L}$, $d^9\underline{L}^2$, and $d^{10}\underline{L}^3$ components (lower panel).

parameters B and C are fixed at 0.142 and 0.527 eV, which are 80% of the atomic HF values.[19,20] Although the values of B and C are slightly different from those obtained from atomic spectroscopy data,[17] the differences do not affect the present conclusion. The crystal field from the nonorthogonality is ~0.57 eV for the ground state. The Pr $3d$ core-level photoemission spectrum is very similar to that of Pr_2O_3,[28] which indicates that the valence of the Pr ion is exactly $3+$. This confirms that the formal valence of Ni is $3+$.

B. Valence band

The valence-band photoemission spectra taken at various photon energies from 40 to 1253.6 eV are shown in Fig. 5. Since the relative photoionization cross section of O $2p$ to Ni $3d$ and Pr $4f$ increases as the photon energy decreases, the structure at 5 eV is dominated by the O $2p$ character and the structure at 1.5 eV is mainly derived from the Ni $2p$ and Pr $4f$ states. In order to extract the Pr $4f$ contribution from the valence-band spectra, we

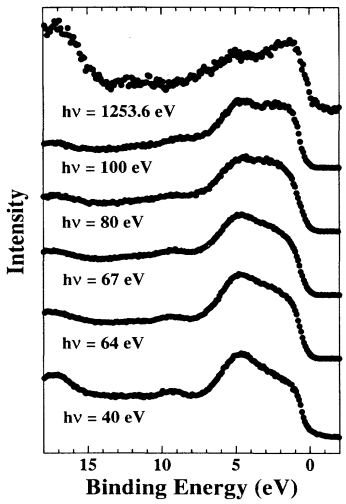

FIG. 5. Valence-band XPS and UPS spectra of $PrNiO_3$ taken at $h\nu=40$, 64, 67, 80, 100, and 1253.6 eV.

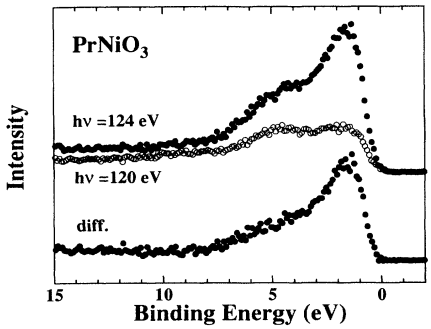

FIG. 6. Pr $4d$-$4f$ resonant-photoemission spectra of $PrNiO_3$ taken with on-resonance ($h\nu=124$ eV, dots) and off-resonance ($h\nu=120$ eV, open circles) photon energies and their difference spectrum (dots).

have measured the Pr $4d$-$4f$ resonant-photoemissin spectra (Fig. 6). By subtracting the off-resonant spectra ($h\nu=120$ eV) from the on-resonant ($h\nu=124$ eV), we obtain the Pr $4f$-derived spectrum as shown in Fig. 6. Here, we have assumed that the intensity distribution of the on-resonant Pr $4f$-derived spectrum is not changed from that of the off-resonant spectrum. Ni $3p$-$3d$ resonant-photoemission spectra have also been measured. The photon energy dependence of the monochromater has been corrected using the photon absorption of Au taken in the total-electron-yield mode. As shown in Fig. 7, the broad satellite structure ranging from 7 to 15 eV is enhanced by the $3p$-$3d$ resonance and can be assigned to a so-called charge-transfer satellite. The intensity of the main-band region ranging from 0 to 5 eV is reduced from 64 to 67 eV because of the reduction of the photoionization cross section of O $2p$. The weak structure at ~ 9.5 eV, which appears in the spectra taken at low photon enegies ($h\nu=40$, 64, and 67 eV), would be from surface contamination.

In analyzing the valence-band XPS spectrum of $PrNiO_3$, we have performed a CI calculation on an octahedral NiO_6^{9-} cluster model including multiplet coupling.[11] After subtracting the background due to secondary electrons, the existence of the broad satellite structure from 8 to 14 eV becomes clear. We have determined the values of Δ, U, and $(pd\sigma)$ in order to reproduce the shape of the spectra including the satellite structure. The result of the CI calculation is compared with the experimental data in Fig. 8. We have added the contribution from the O $2p$ band centered at ~ 5 eV, assuming a Gaussian form, and the Pr $4f$ band obtained from the Pr $4d$-$4f$ resonant photoemission taking into account the relative cross section of these atomic orbitals.[29,30] The best-fit parameters are $\Delta=1.0\pm1.0$ eV, $U=7.0\pm1.0$ eV, and $(pd\sigma)=-1.5\pm0.2$ eV, which are consistent with those obtained from the Ni $2p$ core-level spectrum.

For the present parameter set, the symmetry of the ground state is found to be ${}^2E_g$, namely, the Ni ion is in the low-spin state. The boundary between the high-spin (${}^4T_{1g}$) and low-spin (${}^2E_g$) states is $\Delta\sim 2.0$ eV with the other parameters fixed to the obtained values. The ground state has 34% d^7, 56% $d^8\underline{L}$, and 10% $d^9\underline{L}^2$ character and is strongly covalent. The calculated local magnetic moment in the low-spin state is $0.91\mu_B$, which is close to the purely ionic value and is in good agreement with the neutron-diffraction measurement.[3] The reason why the magnetic moment is close to the ionic value of the low-spin Ni^{3+}, $1\mu_B$, in spite of the strongly covalent ground state is as follows. Let us consider charge transfer to the ionic low-spin configuration $t_{2g}\uparrow{}^3t_{2g}\downarrow{}^3e_g\uparrow$. The charge transfer of an electron whose spin is parallel to the Ni $3d$ local spin is more favored by the intraatomic exchange interaction than that of an electron whose spin is antiparallel to the Ni spin. On the other hand, for an electron with antiparallel spin, two e_g orbitals are available for charge transfer while, for an electron with parallel spin, only one e_g orbital is available. Since

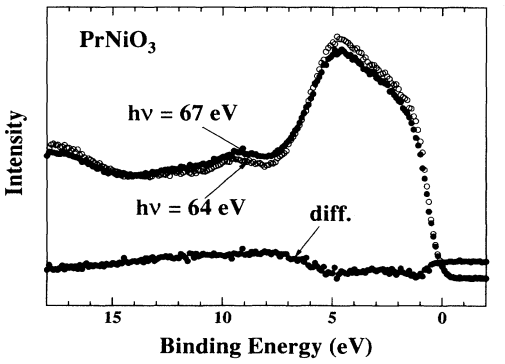

FIG. 7. Ni $3p$-$3d$ resonant photoemission spectra of $PrNiO_3$ taken with on-resonance ($h\nu=67$ eV, dots) and off-resonance ($h\nu=64$ eV, open circles) photon energies and their difference spectrum (dots).

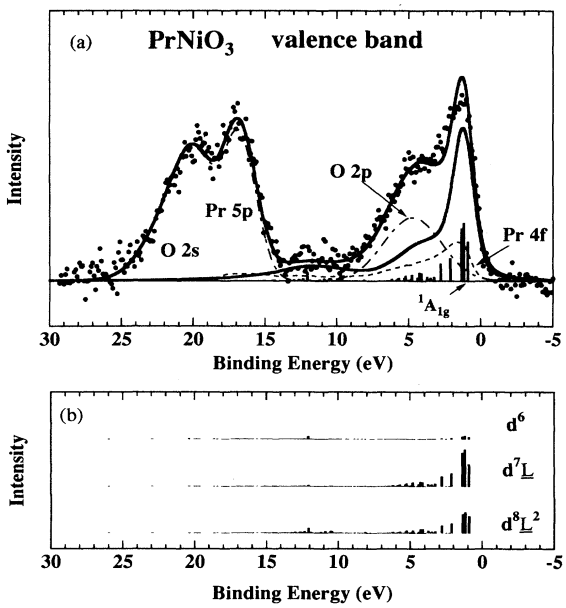

FIG. 8. (a) Cluster-model calculation for valence-band photoemission spectrum compared with the experimental result. (b) The line spectra are decomposed into the d^7, $d^8\underline{L}$, and $d^9\underline{L}^2$ components.

cancel each other, namely, the amount of the charge transfer for the parallel spin is almost equal to that for the antiparallel spin, the net local spin of Ni remains close to the purely ionic one. Actually, 26% of the ground state is of $t_{2g}\uparrow^3 t_{2g}\downarrow^3 e_g\uparrow^2\underline{L}\uparrow$ type and 30% is of $t_{2g}\uparrow^3 t_{2g}\downarrow^3 e_g\uparrow e_g\downarrow\underline{L}\downarrow$ type.

In the final state of valence-band photoemission, $d^7\underline{L}$ character is dominant in the main band at 1.5 eV, and the satellite region has mainly d^6 and $d^8\underline{L}^2$ character. The d^6 character in the satellite region causes enhancement of the satellite intensity in the Ni 3*p*-3*d* resonant photoemission spectrum. The symmetry of the first ionization state is $^1A_{1g}$, which has 5% d^6, 53% $d^7\underline{L}$, and 42% $d^8\underline{L}^2$ character. The first affinity state with $^3A_{2g}$ symmetry is found to be dominated by d^8 character (84% d^8 and 16% $d^9\underline{L}$). Here, let us consider the characters of the excitations from the ground state to the first ionization and affinity states. The *d* and *p* weights of the excitation from the ground state to the first ionization state are given by the differences between the net numbers of *d* and *p* holes in the ground state and those in the first ionization state, respectively. Those of the excitation from the ground state to the first affinity state are also given in the same way. In our cluster-model analysis, the net numbers of the *d* and *p* holes are 2.24 and 0.76 in the ground state, 2.63 and 1.37 in the first ionization state, and 1.84 and 0.16 in the first affinity state, respectively. Therefore the excitation from the ground state to the first ionization state has 39% *d* and 61% *p* character and that from the ground state to the first affinity state has 40% *d* and 60% *p* character. Therefore the band gap of ~2.3 eV obtained by the cluster-model calculation is far from being of *p-d* or charge-transfer type, but has strongly hybridized "*pd-pd*" character.

C. X-ray absorption spectra

The O 1*s* XAS spectrum reflects the O 2*p* weight hybridized into the unoccupied states of the transition-metal and rare-earth ions.[31] The O 1*s* spectrum of $PrNiO_3$ is shown in Fig. 9, and is in good agreement with that measured by Medarde *et al.*[6] The sharp peak at 529 eV is derived from the Ni 3*d* state and the structures ranging from 530 to 545 eV are due to the Pr 4*f* and 5*d* and Ni 4*s* and 4*p* states. If we neglect the effect of the O 1*s* core-hole potential on the unoccupied states, the final state of the O 1*s* XAS can be regarded as the $(N+1)$-electron state, which is equivalent to the final state of inverse photoemission. We have calcualted the O 1*s* XAS spectrum using the cluster model with the above parameter set and have compared it with the experimental result in Fig. 9. Here, we have shifted the calculated O 1*s* XAS spectrum by 1.4 eV towards lower photon energy from the photon energy equal to the O 1*s* binding energy in XPS. According to the calculation, the dominant peak is due to the first affinity level $^3A_{2g}$ and the high-energy tail is derived from ^1E_g and $^1A_{1g}$ states.

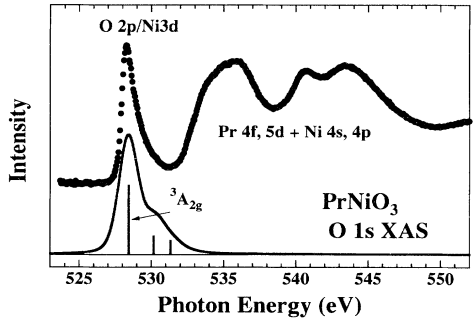

FIG. 9. O 1*s* XAS spectrum of $PrNiO_3$ compared with the cluster-model calculation. The parameters are $\Delta=1.0$ eV, $U=7.0$ eV, and $(pd\sigma)=-1.5$ eV.

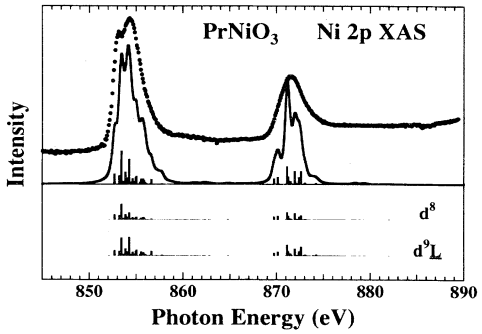

FIG. 10. Ni 2*p* XAS spectrum of $PrNiO_3$ compared with the cluster-model calculation. The parameters are $\Delta=1.0$ eV, $U=7.0$ eV, $(pd\sigma)=-1.5$ eV, and $F^0=9.5$ eV. $Q\equiv F^0-\frac{1}{15}G^1-\frac{3}{70}G^3\approx 9.0$ eV.

In Fig. 10, we have compared the Ni 2*p* XAS spectrum with the full-multiplet cluster-model calculation, which has been obtained by broadening the line spectrum with a Gaussian and a Lorentzian. The FWHM of the Gaussian is ~0.6 eV, which is determined by the energy resolution, and that of the Lorentzian is ~0.5 eV, which is derived from the natural width.[32] The parameters used in this calculation are exactly the same as those for the Ni 2*p* XPS spectra. It has been shown that the double-peak structure of the $2p_{3/2}$ main peak is due to multiplet splitting. Weak and broad satellite structures, which are located on the high-energy side separated by ~5 eV from the main peak, are reproduced to some extent. In order to improve agreement with the experimental results, an extra broadening of the calculated result is necessary. The extra broadening of transition-metal 2*p* XAS has also been observed in mixed-valence compounds such as $Li_{1-x}Ni_xO_2$ (Ref. 33) and $La_{1-x}Sr_xFeO_3$,[34] and has been attributed to the coexistence of several components with different symmetries (in the single-cluster picture) in the ground state. Since $PrNiO_3$ is located at the metal-insulator boundary, it may undergo this type of extra broadening.

D. Unrestricted Hartree-Fock calculations

From the above cluster-model calculations, it has been found that $PrNiO_3$ has a small positive $\Delta\sim 1$ eV and that the d^7 and $d^8\underline{L}$ configurations are strongly hybridized in the ground state. In transition-metal oxides with very

small positive or negative Δ, the magnitude of the band gap is strongly affected by the geometrical arrangement of transition-metal and oxygen ions. Actually, $RNiO_3$ shows a metal-to-insulator transition as a function of the size of the R ion, which controls the magnitude of the $GdFeO_3$-type latice distortion. In order to investigate the relationship between the $GdFeO_3$-type distortion and the metal-to-insulator transition in $RNiO_3$, we have made unrestricted HF calculations on a perovskite-type lattice model.

The magnetic structure of $PrNiO_3$ has been found to be very complicated and to give a large unit cell containing 16 unit formulas. Each Ni spin is ferromagnetically coupled to three nearest-neighbor Ni spins and antiferromagnetically coupled to the other three.[9] In order to explain this unusual magnetic ordering, it has been proposed that the e_g electrons of the low-spin Ni^{3+} ($t_{2g\uparrow}{}^3 t_{2g\downarrow}{}^3 e_{g\uparrow}$) are polarized into the $3z^2-r^2$ and x^2-y^2 orbitals for the ferromagnetically coupled Ni pair and are polarized into one of these orbitals for the antiferromagnetically coupled Ni pair.[9] Since the magnetic structure can be viewed as a mixture of FM and G-, A-, and C-type AFM magnetic arrangments, these four simplified magnetic structures have been studied in Ref. 22, where it has been reported that the high-spin state with G-type AFM ordering has the lowest energy and the low-spin metallic state with FM ordering has the second lowest energy for the realistic parameter set $\Delta=1.0$ eV, $U=7.0$, eV, and $(pd\sigma)=-1.8$ eV. The third lowest solution is the low-spin insulating solution with the A-type AFM arrangment accompanied by a "$3x^2-r^2$"/"$3y^2-r^2$"-type orbital ordering. The reason why the low-spin state is not so stabilized as the high-spin state in the HF approximation may be as follows. A single Slater determinant within the HF approximation can be a good description of the high-spin state but it fails to describe the low-spin state. In particular, for small Δ, a Heitler-London-type wave function $1/\sqrt{2}(|\underline{u}_\uparrow \underline{L}_{u\uparrow} \underline{v}_\uparrow|+|\underline{L}_{u\uparrow} \underline{u}_\uparrow \underline{v}_\uparrow|)$ has a large weight in the ground state, where $\underline{u}$ and $\underline{v}$ represent holes in the $3z^2-r^2$ and x^2-y^2 orbitals, respectively, and $\underline{L}_u$ and $\underline{L}_v$ denote holes in the molecular orbitals with $3z^2-r^2$ and x^2-y^2 symmetries constructed from O $2p$ orbitals, respectively. Therefore the inclusion of this kind of correlation effect will stabilize the low-spin state relative to the high-spin state. In this work, we have done HF calculations for the 16-molecule unit cell with the actual spin arrangement, in which the e_g electrons are polarized into "$3z^2-r^2$" and "x^2-y^2" obitals. The solution has an energy higher by $\sim$50 meV per unit formula than the A-type AFM solution. Further investigations would be required to understand why the complicated magnetic structure is realized in the low-spin $PrNiO_3$.

It is interesting to investigate how far the HF calculation can describe the photoemission spectra or the single-particle excitation spectra. In Fig. 11, the density of states (DOS) for the A-type AFM solution, which is the most stable low-spin and insulating solution for the present parameter set, has been displayed. The shaded area shows the $3d$-derived partial DOS. The $2p$ and $3d$ orbitals are strongly hybridized in the states just below and above the band gap, in good agreement with the cluster-model analysis. This indicates that the HF calculation correctly describes the character of the band gap. In the inset of Fig. 11, we have compared the experimental result with the DOS where the $2p$ and $3d$ partial DOS's have been multiplied by their photoionization cross sections.[29,30] According to the cluster-model analysis, the peak at 1.5 eV of the experimental result is mainly from the t_{2g} state where the Ni $3d$ and O $2p$ characters are strongly hybridized. In the HF calculation, the t_{2g} band is located at 2.5 eV and is shifted toward high binding energy by $\sim$1 eV from the experimental result. The HF calculation also fails to reproduce the satellite structure.

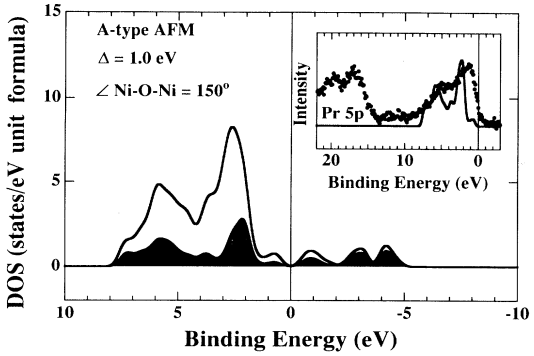

FIG. 11. Total DOS and the Ni $3d$ partial DOS (shaded region) for the A-type AFM state. The DOS obtained by multiplying the O $2p$ and Ni $3d$ partial DOS's by their photoionization cross sections is compared with the experimental result in the inset.

In Fig. 12, we have plotted the magnitude of the band gap as a function of the Ni-O-Ni bond angle. The band gap increases as the $GdFeO_3$-type distortion becomes large for the A-type AFM solutions through the decrease in the intercluster Ni-O-Ni transfer integrals. This explains the observation that the increase of the $GdFeO_3$-type lattice distortion make $RNiO_3$ insulating.[1] Barman, Chainani, and Sarma, on the other hand, attributed the origin of the metallic behavior of $LaNiO_3$ versus the insulating behavior of $NdNiO_3$ to the difference in the magnitude of the O $2p$–to–Ni $3d$ transfer integral:[7] Metallic $LaNiO_3$ has larger transfer integrals than insulating $NdNiO_3$. They also claimed that pressure causes an increase of the transfer integral and causes $NdNiO_3$ to be-

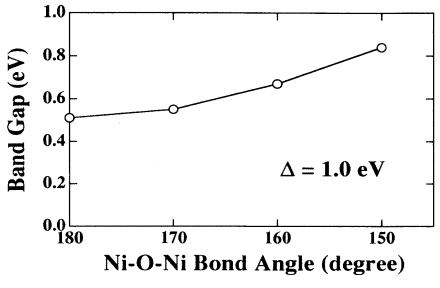

FIG. 12. Calculated magnitude of the band gap as a function of the $GdFeO_3$-type lattice distortion.

come metallic. A neutron-diffraction study under pressure will be able to determine whether the intracluster change or intercluster change is responsible for the metal-insulator transition.

V. CONCLUDING REMARKS

By analyzing the photoemission spectra of $PrNiO_3$ using the cluster model, Δ is estimated to be ~ 1 eV. In the ground state, the d^7 configuration is strongly hybridized with the $d^8\underline{L}$ configuration. However, the local magnetic moment is calculated to be $0.9\mu_B$, which is close to the ionic value and is in good agreement with the neutron-diffraction measurement.[3] A HF calculation using the parameters from the cluster-model analyses has shown that the $GdFeO_3$-type lattice distortion enlarges the magnitude of the band gap. The lattice distortion strongly affects the band gap of $PrNiO_3$, which has a small Δ and a covalent ground state.

In the present work, we have studied the electronic structure of $PrNiO_3$ by two theoretical approaches: a local cluster calculation and a HF band-structure calculation. The comparison of the two extremes gives us a clue to understand how strongly correlation effect, especially the Heitler-London type effect, affect the metallic versus insulating behavior of $PrNiO_3$. On one hand, as shown in the previous section, HF calculations can give us a crude but useful picture of the metal-to-insulator boundary. The opening of band gaps for small, positive Δ has been discussed by Sarma[35] in terms of the strong covalency in the ground state and these compounds have been called "covalent insulators." Following it, Nimkar, Sarma, and Krishnamurthy studied the metal-insulator boundary for the CuO_2 plane using the unrestricted HF approximation.[25] The HF result, which does not include the Heitler-London-type correlation effect, matches the view of the "covalent" insulator. On the other hand, the local cluster approach, where the intracluster Heitler-London-type correlations are exactly taken into account, can reproduce the various spectra, suggesting that electron correlation within the local cluster is important. Key questions are how strong the Heitler-London-type correlation is in the vicinity of the metal-insulator boundary and how far the picture of the local cluster model can survive in the real lattice. Since the HF calculation cannot reproduce the satellite structure of the valence-band photoemission spectra, it is necessary to see how the HF ground state is affected by the correlation effect when one attempts to reproduce the photoemission spectra.

ACKNOWLEDGMENTS

The authors would like to thank A. Yagishita of Photon Factory and the staff of Synchrotron Radiation Laboratory for technical support. They are grateful to H. Namatame, K. Morikawa, T. Saitoh, A. Sekiyama, I. H. Inoue, and M. Nakamura for assistance in the XAS measurement, and to T. Yagi, T. Uchida, and T. Hishinuma for help in preparing the samples. They would also like to thank M. Abbate, D. D. Sarma, and V. I. Anishimov for valuable discussions. All the calculations in this work were performed on a VAX computer in Meson Science Laboratory, Faculty of Science, University of Tokyo. The present work is supported by a Grant-in-Aid for Scientific Research from the Ministry of Education, Science and Culture and by the New Energy and Institute Technology Development Organization (NEDO). Part of this work has been done under the approval of the Photon Factory Program Advisory Committee (Proposal No. 92-141).

[1]P. Lacorre, J. B. Torrance, J. Pannetier, A. I. Nazzal, P. W. Wang, and T. C. Huang, J. Solid State Chem. **91**, 225 (1991); J. B. Torrance, P. Lacorre, A. I. Nazzal, E. J. Ansaldo, and C. H. Niedermayer, Phys. Rev. B **45**, 8209 (1992); J. L. García-Muñoz, J. Rodríguez-Carvajal, P. Lacorre, and J. B. Torrance, *ibid.* **46**, 4414 (1992).

[2]J. B. Goodenough and P. Raccah, J. Appl. Phys. **36**, 1031 (1965).

[3]J. L. García-Muñoz, J. Rodríguez-Carvajal, and P. Lacorre, Europhys. Lett. **20**, 241 (1992); Phys. Rev. B **50**, 978 (1994).

[4]J. Zaanen, G. A. Sawatzky, and J. W. Allen, Phys. Rev. Lett **55**, 418 (1985); J. Zaanen and G. A. Sawatzky, Can. J. Phys. **65**, 1262 (1987); J. Solid State Chem. **88**, 8 (1990); S. Hüfner, Z. Phys. B **61**, 135 (1985).

[5]T. Mizokawa, H. Namatame, A. Fujimori, K. Akeyama, H. Kondoh, H. Kuroda, and N. Kosugi, Phys. Rev. Lett. **67**, 1638 (1991); **70**, 1565(E) (1993); Phys. Rev. B **49**, 7193 (1994); A. E. Bocquet, A. Fujimori, T. Mizokawa, T. Saitoh, H. Namatame, S. Suga, N. Kimizuka, Y. Takeda, and M. Takano, *ibid.* **45**, 1561 (1992); D. D. Sarma, H. R. Krishnamurthy, S. Nimkar, S. Ramasesha, P. P. Mitra, and T. V. Ramakrishnan, Pramana J. Phys. **38**, L531 (1992).

[6]M. Medarde, A. Fontaine, J. L. García Muñoz, J. Rodríguez-Carvajal, M. de Santis, M. Sacchi, G. Rossi, and P. Laccore, Phys. Rev. B **46**, 14 975 (1992).

[7]S. R. Barman, A. Chainani, and D. D. Sarma, Phys. Rev. B **49**, 8475 (1994).

[8]T. Arima, Y. Tokura, and J. B. Torrance, Phys. Rev. B **48**, 17 006 (1993).

[9]M. Abbate, F. M. F. de Groot, J. C. Fuggle, A. Fujimori, O. Strebel, F. Lopez, M. Domke, G. Kaindl, G. A. Sawatzky, M. Takano, Y. Takeda, H. Eisaki, and S. Uchida, Phys. Rev. B **46**, 3771 (1992).

[10]M. Grioni, J. B. Goedkoop, R. Schoorl, F. M. F. de Groot, J. C. Fuggle, F. Schäfers, E. E. Koch, G. Rossi, J.-M. Esteva, and R. C. Karnatak, Phys. Rev. B **39**, 1541 (1989).

[11]A. Fujimori and F. Minami, Phys. Rev. B **30**, 957 (1984).

[12]J. Zaanen, C. Westra, and G. A. Sawatzky, Phys. Rev. B **33**, 8060 (1986).

[13]J. C. Slater and G. F. Koster, Phys. Rev. **94**, 1498 (1954).

[14]W. A. Harrison, *Electronic Structure and the Properties of Solids* (Dover, New York, 1989).

[15]L. F. Mattheiss, Phys. Rev. B **5**, 290 (1972).

[16]S. Sugano, Y. Tanabe, and H. Kamimura, *Multiplets of Transition Metal Ions in Crystals* (Academic, New York, 1970).

[17]J. B. Mann (unpublished).

[18]A. E. Bocquet, T. Mizokawa, T. Saitoh, H. Namatame, and A. Fujimori, Phys. Rev. B **46**, 3771 (1992).
[19]K. Okada and A. Kotani, J. Phys Soc. Jpn. **60**, 772 (1991); **61**, 4619 (1992).
[20]F. M. F. deGroot, J. C. Fuggle, B. T. Tole, and G. A. Sawatzky, Phys. Rev. B **42**, 5459 (1990).
[21]T. Mizokawa and A. Fujimori, Phys. Rev. B **48**, 14 150 (1993).
[22]O. Gunnarsson and O. Jepsen, Phys. Rev. B **38**, 3568 (1988).
[23]T. Mizokawa and A. Fujimori, Phys Rev. B **51**, 12 880 (1995).
[24]M. Cyrot and C. Lyon-Caen, J. Phys. (Paris) **36**, 253 (1975).
[25]S. Nimkar, D. D. Sarma, and H. R. Krishnamurthy, Phys. Rev. B **47**, 10 927 (1993).
[26]J. Kanamori, Prog. Theor. Phys. **30**, 275 (1963).
[27]E. R. Gagliano and C. A. Balseiro, Phys. Rev. B **38**, 11 766 (1988).
[28]H. Ogasawara, A. Kotani, R. Potze, G. A. Sawatzky, and B. T. Thole, Phys. Rev. B **44**, 5465 (1991).
[29]J. J. Yeh and I. Lindau, At. Data Nucl. Data Tables **32**, 1 (1985).
[30]Here, we have artificially multiplied the photoionization cross section of the O 2*p* subshell by a factor of 3, which has been empirically found in previous studies. The XPS study of V_2O_3 by Sawatzky and Post [Phys. Rev. B **20**, 1546 (1979)] also shows that the intensity ratios of O 2*p* to O 2*s* and to V 3*d* are three times larger than those calculated.
[31]F. M. F. de Groot, M. Grioni, J. C. Fuggle, J. Ghijsen, G. A. Sawatzky, and H. Petersen, Phys. Rev. B **40**, 5715 (1989).
[32]M. O. Krause and J. H. Oliver, J. Phys. Chem. Ref. Data **8**, 329 (1979).
[33]J. van Elp, B. G. Searle, G. A. Sawatzky, and M. Sacchi, Solid State Commun. **80**, 67 (1991).
[34]M. Abbate, F. M. F. de Groot, J. C. Fuggle, A. Fujimori, O. Strebel, F. Lopez, M. Domke, G. Kaindl, G. A. Sawatzky, M. Takano, Y. Takeda, H. Eisaki, and S. Uchida, Phys. Rev. B **46**, 4511 (1992).
[35]D. D. Sarma, J. Solid State Chem. **88**, 45 (1990).